

Corrosion Inhibition of Mild Steel by Benzopyranone Derivative in 1.0 M HCl Solutions

Jiajun Fu¹, Junyi Pan², Zhuo Liu¹, Suning Li¹, Ying Wang^{*}

¹School of Chemical Engineering, Nanjing University of Science and Technology, Nanjing 210094, P. R. China

²Department of Earth Sciences, Nanjing University, Nanjing 210093, P. R. China

*E-mail: fujiajun668@gmail.com

Received: 12 April 2011 / Accepted: 15 May 2011 / Published: 1 June 2011

A new corrosion inhibitor namely N-((7-acetoxy-2-oxo-2H-1-benzopyran-4-yl) methyl)-2-(acryloyloxy)-N,N-dimethylethanaminium bromide (AOBAB) has been synthesized and its influences on corrosion inhibition of mild steel in 1.0 M HCl solutions have been studied by weight loss measurement, electrochemical impedance spectroscopy (EIS), Tafel polarization technique and scanning electron microscope (SEM). According to all the experimental results, the inhibition efficiency increases with increase in the concentrations of AOBAB, and also increases with increase in temperature. Tafel polarization studies revealed that the AOBAB acts as a mixed inhibitor. Adsorption of AOBAB on the mild steel surface in 1.0 M HCl solutions follows the Langmuir isotherm model. The activation energy and the thermodynamic parameters, such as apparent activation energy (E_a), enthalpy of activation (ΔH^*) and entropy of activation (ΔS^*), adsorption equilibrium constant (K_{ads}), standard free energy of adsorption (ΔG_{ads}) for the inhibition process were also calculated. SEM observations of the mild steel surface confirmed that inhibitor molecules strongly adsorbed onto the surface.

Keywords: Benzopyranone, mild steel, electrochemical measurement, adsorption

1. INTRODUCTION

Mild steel, the most widely used engineering material, corrode in many circumstances, especially in some industrial processes, such as acid cleaning, acid descaling and oil well acidizing [1-3]. The use of inhibitors is one of the most practical and economical methods to reduce the corrosive attack on metal materials. It is well-known that the most effective acidic corrosion inhibitors for many metals and alloys are organic compounds containing electronegative atoms (nitrogen, sulfur, oxygen, phosphor etc.), unsaturated bonds (such as double or triple bonds, etc.) and aromatic or heterocyclic

rings [4-7]. It has been established that the adsorption of these organic compounds at the metal solution interface is the first step in the mechanism of the inhibitory action [8]. Generally speaking, two types of interaction are responsible for adsorption of inhibitor to metal surface. One is physisorption, which requires the presence of both electrically charged metal surface and charged species on the bulk of the solution. The other is chemisorption, which involves direct adsorption on the basis of donor-acceptor interactions between the lone pairs of electron, π -electrons and the vacant d-orbitals of iron surface atoms [9, 10]. It has been observed that adsorption extent depends mainly on some physicochemical properties of the inhibitor molecule, such as its distribution of charge density, the molecular size, the number of adsorption-active centers, the formation of metallic complexes and so on [11].

In recent years, with improved recognition of environmental protection, a new generation of heterocyclic compounds regarding as green corrosion inhibitors has attracted the increased attention of researchers. Several reports have documented the use of many synthetic heterocyclic compounds, such as benzothiazolic quaternary ammonium bromides, pyridinium derivatives, pyrimidine derivatives and oxo-triazole derivatives as effective corrosion inhibitors in acidic media [12-16]. Benzopyranone derivatives as an important class of organic heterocyclic compound have been reported to have multiple physiological activities, such as antibacterial, antifungal, disinfection, anticoagulant and antitumor properties [17, 18]. However, to the best of our knowledge, data regarding the using of Benzopyranone derivatives as corrosion inhibitors are still scarce. Şahin et al. studied the corrosion inhibition activity of three heterocyclic compounds namely 3-amino-1,2,4-triazole, 4-hydroxy-2H-1-benzopyran-2-one and 4-hydroxy-3-(1H-1,2,4-triazole-3-ylazo)-2H-1-benzopyran-2-one as corrosion inhibitor for mild steel in 3.5% NaCl media and reported them as potential inhibitors [19]. In the present work, newly synthesized Benzopyranone derivative namely N-((7-acetoxy-2-oxo-2H-1-benzopyran-4-yl) methyl)-2-(acryloyloxy)-N,N-dimethylethanaminium bromide (AOBAB) was studied as potential corrosion inhibitor for mild steel in 1.0 M HCl solutions. The chemical structure of AOBAB is given in Fig. 1.

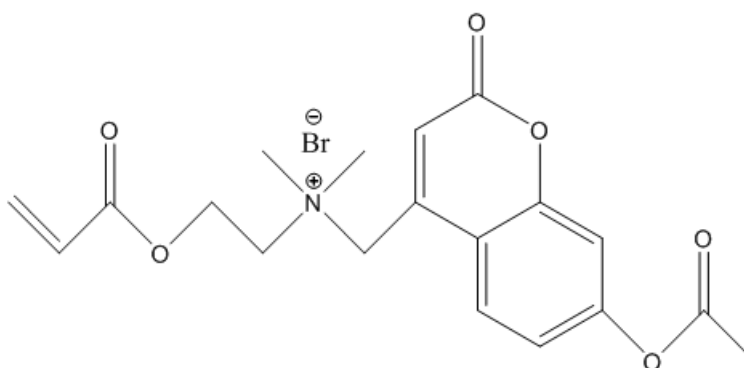


Figure 1. Chemical molecular structure of AOBAB

The choice of AOBAB used as corrosion inhibitor is based on the following analyses: (a) AOBAB possess multiple adsorption centers such as positive quaternary ammonium ion, aromatic

ring, conjugated double bonds and heteroatom in pyrone, which facilitate the adsorption of the inhibitor onto the metal surface. (b) AOBAB has a high molecular weight (the molecule is 508.4 g/mol) and likely to effectively cover more surface area via adsorption (c) AOBAB has high solubility in aqueous solutions, especially in acid solutions. Hence, AOBAB is expected to be a good corrosion inhibitor. Then, the weight loss measurement, Tafel polarization technique and electrochemical impedance spectroscopy (EIS) were performed to evaluate the inhibition efficiency of AOBAB. The thermodynamic parameters for corrosion process were also calculated and discussed. Finally, the surface morphology study was used to establish good corrosion protection of the compounds.

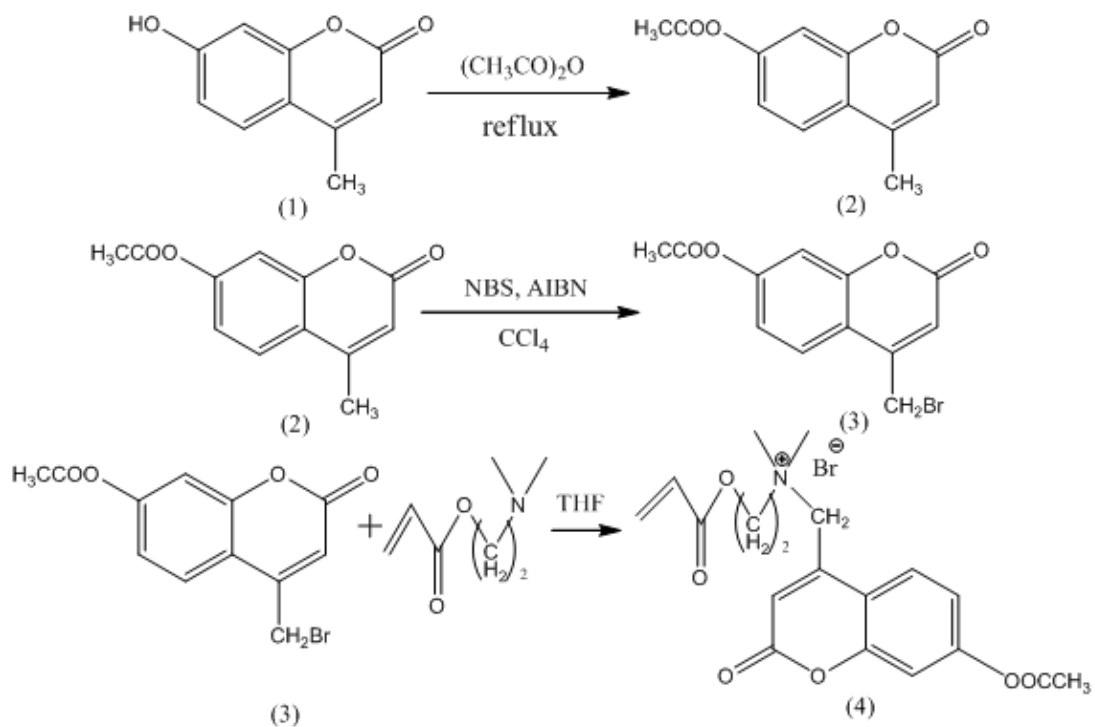
2. EXPERIMENTAL

2.1. Synthesis process of AOBAB

Scheme 1 summarized the method of synthesis of AOBAB. It was prepared through three steps. The structure of intermediate and final products was confirmed by $^1\text{H-NMR}$ and FT-IR spectroscopic methods.

(1) Synthesis of 7-acetyloxy-4-methyl-2H-1-Benzopyran-2-one (2)

A mixture of 1.76 g (0.01 mol) of 7-hydroxy-4-methyl-2H-1-Benzopyran-2-one (1) and 3.57 g (0.035 mol) acetic anhydride were mixed and refluxed in an oil bath for about 2 h.



Scheme 1. Preparation of AOBAB

After the solution was cooled to room temperature, pouring the solution into ice water bath resulted in the formation of a large amount of white precipitate. The collected solid was washed thoroughly with distilled water and then recrystallized from anhydrous alcohol to afford pure compound 7-acetyloxy-4-methyl-2H-1-Benzopyran-2-one (**2**).

IR (KBr) / ν (cm⁻¹): 3053 (=C-H stretching), 2937 (-CH₃, stretching), 1764 (-C=O, stretching), 1209 (C-O-C, asymmetric stretching), 850 (-C=C-, bending vibration).

¹H-NMR (300MHz) /DMSO/ δ ppm: 2.29 (s, 3H, CH₃-C(=O)-O-), 2.41 (s, 3H, CH₃-C=CH-C(=O)-O-), 6.37 (s, 1H, CH₃-C=CH-C(=O)-O-), 7.15~7.18 (d, 1H, -O-C=CH-CH=C-), 7.25 (-O-C-CH=C-O-), 7.78~7.81 (d, -O-C=CH-CH=C-).

(2) Synthesis of 7-acetyloxy-4-bromomethyl-2H-1-Benzopyran-2-one (**3**)

1.75 g (0.009mol) of 7-acetyloxy-4-methyl-2H-1-Benzopyran-2-one (**2**) and a small amount of initiator azobisisobutyronitrile (AIBN) were added dropwise to the 1.78 g (0.01mol) n-bromosuccinimide dispersed on carbon tetrachloride (40 ml) and the mixture was refluxed for 20 h. After cooling to the room temperature, the solvent was removed by vacuum distillation.

The residuals were extracted by washing (water), filtered and dried to yield the crude products, 7-acetyloxy-4-bromomethyl-2H-1-Benzopyran-2-one (**3**), which were purified by recrystallization from ethyl acetate.

IR (KBr) / ν (cm⁻¹): 1760 (-C=O, stretching), 1203 (-C-O-C-, asymmetric stretching), 1124 (C-O-C, stretching), 859 (-C=C-, bending vibration), 582 (C-Br, stretching).

¹H-NMR (300MHz) /DMSO/ δ ppm: 2.29 (s, 3H, CH₃-C(=O)-O-), 4.87 (s, 2H, Br-CH₂-C=CH-C(=O)-O-), 6.71 (s, 1H, Br-CH₂-C=CH-C(=O)-O-), 7.21~7.23 (d, 1H, -O-C=CH-CH=C-), 7.29 (s, 1H, -O-C-CH=C-O-), 7.90~7.92 (d, 1H, -O-C=CH-CH=C-).

(3) Synthesis of AOBAB (**4**)

A solution of 1.36 g (0.005 mol) 7-(acetyloxy)-4-(bromomethyl)-2H-1-Benzopyran-2-one (**3**) in N,N-dimethylformamide (5 ml) was slowly added to a solution of 0.69 g (0.0048mol) of N,N-Dimethylaminoethyl acrylate in tetrahydrofuran (20 mL). The mixture was refluxed for 2 h. After cooling to the room temperature, the white granular solid, AOBAB, was filtered off.

IR (KBr) / ν (cm⁻¹): 2956 (-CH₂-, stretching), 1650 (-CO-C=C-, stretching), 1620 (CH₂=CH-, stretching), 1404 (C-N, stretching), 1203 (-C-O-C-, asymmetric stretching).

¹H-NMR (300MHz) /DMSO/ δ ppm: 2.31 (s, 3H, CH₃-C(=O)-O-), 3.21 (s, 6H, CH₃-N-CH₃), 3.98 (t, 2H, -C(=O)-O-CH₂-CH₂-), 4.85 (t, 2H, -C(=O)-O-CH₂-CH₂-), 5.01 (s, 2H, N-CH₂-C=C-), 6.05~6.08 (d, 1H, CH₂-CH-), 6.22~6.31 (m, 1H, CH₂-CH-), 6.41~6.47 (d, 1H, CH₂-CH-), 6.68 (s, 1H, N-CH₂-C=CH-), 7.26~7.27 (d, 1H, N-CH₂-C-C-CH=CH-), 7.40 (s, 1H, -C(=O)-O-C-CH=C-), 8.31~8.34 (d, 1H, N-CH₂-C-C-CH=CH-).

2.2. Medium

The aggressive acid solutions of 1.0 M HCl were prepared by dilution of an analytical grade 37% HCl with double distilled water. The concentration range of AOCAB was from 0.01mM to 1mM in 1.0 M HCl solutions used for corrosion measurements.

2.3. Materials

The chemical composition of mild steel sheet was listed in Table 1. The mild steel sheets used in the weight loss measurements were cut into coupons of dimension $2.5 \times 2.0 \times 0.05$ cm. The same types of sheets were used for the electrochemical measurements. The working electrode was in the form of a rod machined into a cylindrical form embedded in epoxy resin leaving an open surface area of 0.5 cm^2 . Before both measurements, the mild steel coupons were abraded with emery paper (600, 1000, 1200, 2000 grit), then cleaned double distilled water, degreased with acetone, and dried.

Table 1. Chemical composition of mild steel sheet (wt. %)

C	Si	Mn	P	S	Cr	Cu
0.17	0.46	0.46	0.05	0.017	0.08	0.019

2.4. Weight loss measurements

The polished and pre-weighted specimens were suspended in 500 ml 1.0 M HCl solutions containing different AOBAB concentrations at the definite time interval of 4 h in the investigated temperature range. Afterward, the specimens were removed, rinsed with water, degreased with acetone, dried, and then weighed. Triplicate specimens were used in each case and the mean value of the weight loss was recorded. The standard deviation of the observed weight loss was $\pm 1\%$. The corrosion rate (CR) was calculated from the following equation:

$$CR = \frac{W_1 - W_2}{S \times t} \quad 1$$

Where W_1 is the mass of the specimen before immersion in (mg), W_2 is the mass of the specimen after immersion in (mg), S is the total area of the mild steel specimen in (cm^2), t is the corrosion time in (h) and CR is the corrosion rate in ($\text{mg cm}^{-2} \text{ h}^{-1}$).

The percent inhibition efficiency ($IE_w, \%$) was calculated using the following equation:

$$IE_w, \% = \frac{CR_0 - CR}{CR_0} \times 100 \quad 2$$

Where CR_0 and CR are the corrosion rates of the coupon in 1.0 M HCl solutions without and with the addition of AOBAB, respectively.

2.5. Electrochemical measurements

Electrochemical measurements were performed in a conventional three-electrode cell with a capacity 500 ml. The working electrode, a reference saturated calomel electrode (SCE) and platinum

counter electrode of 1.0 cm² were placed inside a three-electrode cell. A fine Luggin capillary was placed close to the working electrode to minimize ohmic resistance. All test solutions were de-aerated in the cell by using pure nitrogen for 30 min prior to the experiment. Measurements were performed at room temperature, 298K with potentiostat (EG&G model 2273). Polarization scans were carried out by changing the electrode potential automatically from -250 to +250 mV with respect to the open circuit potential (OCP) with a scan rate of 0.166 mV/s. Electrochemical impedance spectroscopy studies were carried out in a frequency range of 100 kHz-0.1 Hz using an amplitude of 10mV peak to peak using AC signal at the open circuit potential. The data were collected using PowerSuite software and interpreted with Zsimpwin software. All the electrochemical experiments were measured after immersion of working electrode for 30min in 1.0 M HCl solutions in absence and presence of various concentrations of AOBAB until a steady-state OCP was obtained.

2.6. Scanning electron microscopy (SEM)

The surface morphology of the mild steel specimens was examined after polishing and after exposure to 1.0 M HCl solutions in the absence and presence of a certain concentration of AOBAB using scanning electron microscope (JEOL JSM-6380LV, Japan) at an acceleration voltage of 30 kV. All micrographs of the corroded specimens were carried out at a magnification of 1000×.

3. RESULTS AND DISCUSSION

3.1. Polarization curves

The polarization curves for mild steel in 1.0 M HCl solutions at various concentrations of AOBAB at 298K were shown in Fig. 2. Both cathodic and anodic reactions of mild steel electrode corrosion are inhibited by AOBAB in 1.0 M HCl solutions, which suggests that the addition of AOBAB reduces the mild steel dissolution as well as retards the hydrogen evolution reaction. This may be ascribed to adsorption of inhibitor over the corroded surface.

Electrochemical corrosion kinetics parameters, i.e. corrosion potential (E_{corr}), the cathodic Tafel slope (β_c), anodic Tafel slope (β_a), the inhibition efficiency (IE_p) and corrosion current density (j_{corr}) estimated from intercept of cathodic and anodic Tafel lines were collected in Table 2. In this case, the inhibition efficiency was calculated as follows:

$$IE_p (\%) = \frac{j_{\text{corr}} - j_{\text{corr(inh)}}}{j_{\text{corr}}} \times 100 \quad 3$$

Where j_{corr} and $j_{\text{corr(inh)}}$ are the corrosion current density without and with addition of the inhibitor, respectively. As is evident from the data presented in Table 2, j_{corr} values decrease considerably with increasing the concentration of AOBAB. Additionally, IE_p (%) values increase with the concentration of AOBAB. The highest inhibition efficiency is 96.1% at concentration of 1mM. It can be observed that addition of AOBAB causes more negative shift in E_{corr} , especially in high concentrations.

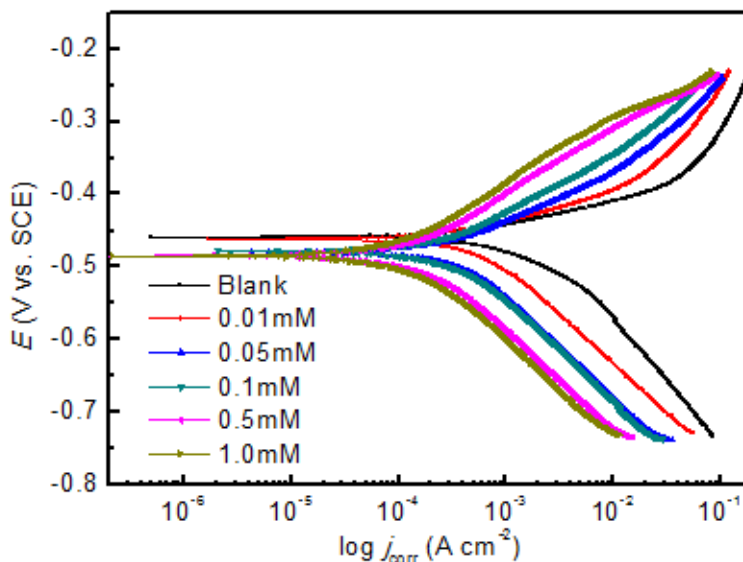


Figure 2. Polarization curves for mild steel in 1.0 M HCl with different concentrations of AOBAB at 298K.

According to the theory of Ferreira [20], if the displacement in corrosion potential is more than 85mV with respect to corrosion potential of the blank, the inhibitor can be seen as a cathodic or anodic type. In this case, the maximum displacement was 26.4 mV. Therefore, AOBAB can be arranged as mixed-type inhibitor in 1.0 M HCl solutions, which suppresses both anodic and cathodic reactions by blocking the reaction sites of iron surface. However, the effect of addition of AOBAB on the cathodic reaction is more pronounced than that on the anodic reaction. Moreover, the anodic Tafel slope values increase in the presence of AOBAB while the cathodic Tafel slope values remain more or less identical, which indicate that the hydrogen evolution is activation-controlled and the reduction mechanism is not affected by the presence of the inhibitors. The increasing in the anodic Tafel slope β_a may be due to the chloride ions/or inhibitor molecules adsorb onto steel surface, and thus increase the energy barrier [21].

Table 2. Electrochemical parameters and inhibition efficiencies of steel corrosion in 1.0 M HCl solutions containing different concentrations of AOBAB at 298K.

Inhibitor	Conc. (mM)	E_{corr} (mV/SCE)	$-\beta_c$ (mV dec ⁻¹)	β_a (mV dec ⁻¹)	I_{corr} ($\mu\text{A cm}^{-2}$)	θ	IE_p (%)
AOBAB	Blank	-458.4	147.2	43.6	919	—	—
	0.01	-461.3	137.7	74.3	372	0.595	59.5
	0.05	-478.6	142.2	83.3	202	0.780	78.0
	0.1	-478.2	146.9	89.9	177	0.807	80.7
	0.5	-484.6	140.8	89.3	74	0.919	91.9
	1.0	-484.8	132.2	82.9	36	0.961	96.1

3.2 Electrochemical impedance spectroscopy (EIS)

Electrochemistry impedance spectroscopy (EIS) is a powerful analysis technique, which can be used to determine the characteristics and kinetics of electrochemical processes occurring at the metal/aggressive media interfaces. The corrosion behaviors of mild steel in 1.0 M HCl solutions in the absence and presence of different concentrations of AOBAB were investigated by EIS at 298K. The impedance responses of the corrosion system are given in Fig. 3 in Nyquist and Bode formats, respectively. As seen from Fig. 3, the Nyquist plots consist of one depressed semicircle with a considerable deviation from an ideal semicircle and the diameter of semicircle increases with increasing inhibitor concentration. The existence of the same shape single semicircles shows the presence of a single charge transfer process during dissolution which is unaffected by the presence of inhibitor molecules. The unperfected semicircle is generally attributed to the inhomogeneities and impurities of the solid electrode surface [22].

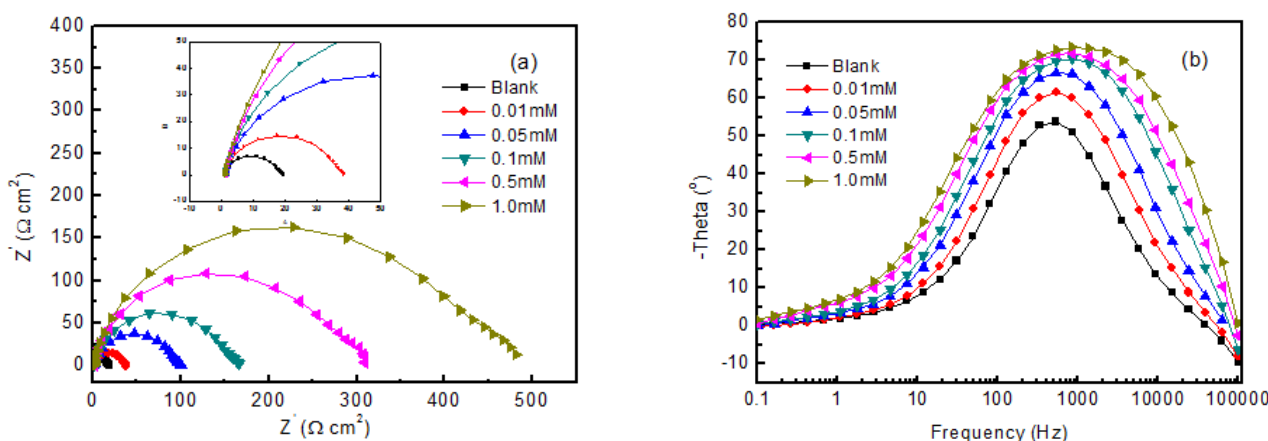


Figure 3. Nyquist (a) and Bode (b) plots for mild steel in 1.0 M HCl solutions without and with different concentrations of AOBAB at 298K

The impedance spectra for Nyquist plots were analyzed by fitting to the classical equivalent circuit model shown in Fig. 4, which has been used previously to model the iron/acid interface. In this classic equivalent circuit, R_s is the solution resistance, R_{ct} is the charge transfer resistance and CPE is a constant phase element. In this case, the constant phase element, CPE is introduced in the circuit instead of a pure double layer capacitor to fit more accurately the behavior of the electrical double layer. CPE is defined in impedance representation as following:

$$Z(\omega) = Z_0 \cdot (j\omega)^{-n} \tag{4}$$

Where Z_0 is the CPE constant, ω is the angular frequency (in rad/s), j is the imaginary unit and n is the CPE exponent. In the CPE, the values of n can be: 1, 0.5, 0 and -1, therefore the CPE

corresponds to different electrical elements: a capacitor, infinite Warburg impedance, resistor and inductor, respectively.

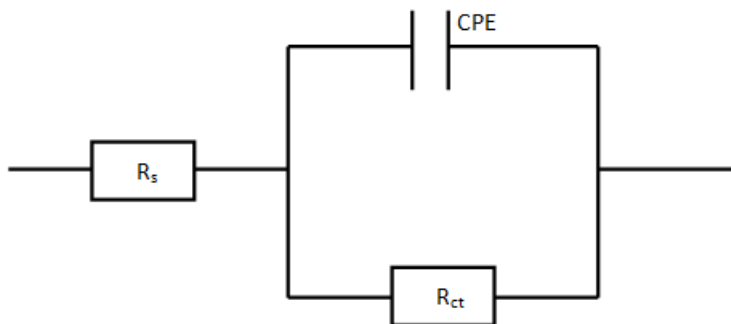


Figure 4. Equivalent circuit model for the studied inhibitors

The impedance parameters, including R_s , R_{ct} and CPE were listed in Table 3. The values of IE_E (%) got from the charge-transfer resistances were calculated using the following equation:

$$IE_E (\%) = \frac{R_{ct}^i - R_{ct}^0}{R_{ct}^0} \times 100 \tag{5}$$

Where R_{ct}^i and R_{ct}^0 are charge transfer resistances in presence and absence of inhibitor, respectively. It is clearly from Table 3, the R_{ct} values increase with the concentration of AOBAB, and this in turn leads to an increasing in IE_E (%). The increase in R_{ct} values is attributed to the formation of protective film on the metal/solution interface, which prevents the mass and charge transferring. On the other hand, the C_{dl} values decrease with an increase in inhibitor concentration. The decrease in C_{dl} is attributed to the decrease in local dielectric constant and/or increase in thickness of surface film layer by the adsorption of the inhibitor molecules on the metal-solution interface. The thickness of the protective layer, e , was associated with C_{dl} according to the Helmholtz model [23]:

$$C_{dl} = \frac{\epsilon_0 \epsilon_r}{e} S \tag{6}$$

Where ϵ_0 is the vacuum permittivity, ϵ_r is the relative permittivity of the material adsorbed on the metallic surface, S is the area covered by the adsorbate and e is the thickness of the coverage film. The parameter n is generally accepted to be a measure of surface inhomogeneity, and its decrease in the inhibited solution compared to the pure acid is connected with an increase in heterogeneity resulting from inhibitor adsorption. In this case, the value of n is close to 1, which means the CPE basically obey the capacitive behavior and therefore Z_0 was substituted with double layer capacitance C_{dl} .

Table 3. Impedance parameters for mild steel in 1.0 M HCl solutions in the absence and presence of different concentrations of AOBAB at 298K.

Conc. (mM)	R_s ($\Omega \text{ cm}^2$)	C_{dl} ($\mu\text{F cm}^2$)	n	R_{ct} ($\Omega \text{ cm}^2$)	η (%)
Blank	1.21	182	0.901	17.5	—
0.01	1.16	115	0.900	36.1	51.52
0.05	1.32	69.4	0.884	94.7	81.52
0.1	1.08	49.1	0.887	157	88.85
0.5	1.13	40.2	0.873	291	93.98
1.0	0.97	32.0	0.872	444	96.06

From the Bode-phase plot ($\log f$ vs. Theta), it is only one time constant, which indicates the AOBAB molecules adsorbed on metal surface by the gradual replacement of water molecules and ions, and not formed a compact film for protection against corrosion. Furthermore, increasing the concentration of AOBAB in the 1.0 M HCl solutions results in more negative values of phase angle at high frequencies, indicating that there was greater surface coverage and transfer charge resistance.

3.3. Weight loss measurements

3.3.1. Effect of inhibitor concentration and expose time

The corrosion of mild steel in 1.0 M HCl in the absence and presence of different concentrations of AOBAB was studied by weight loss measurements. Table 4 shows the corrosion parameters such as, corrosion rate, CR ($\text{mg cm}^{-2} \text{ h}^{-1}$), inhibition efficiency, IE_w (%), and the degree of surface coverage, θ for the mild steel in 1.0 M HCl solutions after 4 h immersion. It is clear that the corrosion rate decreases and the inhibition efficiency increases as inhibitor concentration increased from 0.01 to 1.0 mM. The inhibition action of AOBAB can be attributed to the adsorption of the AOBAB molecules at the iron/acid solution interface. The results obtained from the weight-loss measurements are in good agreement with those obtained from the Tafel polarization measurement and EIS method.

Table 4. Corrosion parameters for mild steel in 1.0 M HCl in the absence and presence of different concentration of AOBAB at 298K

Conc. (mM)	Corrosion rate ($\text{mg cm}^{-2} \text{ h}^{-1}$)	Surface Coverage, θ	IE_w (%)
Blank	5.15	—	—
0.01	2.70	0.476	47.6
0.05	1.43	0.722	72.2
0.1	0.74	0.856	85.6
0.5	0.51	0.901	90.1
1.0	0.41	0.920	92.0

A plot of weight loss vs. time for mild steel in 1.0 M HCl containing various concentrations of AOBAB at 298K is presented in Fig. 5. Fig. 5 reveals that the weight loss of mild steel in 1.0 M HCl solutions increases with increase in the exposure time but decreases with increase in the concentration of AOBAB. It is generally believed that increasing the inhibitor concentration increases the surface coverage of metal surface by inhibitor molecules, which reduces the contact between the metal surface and the aggressive medium and consequently decreases the dissolution of the metal.

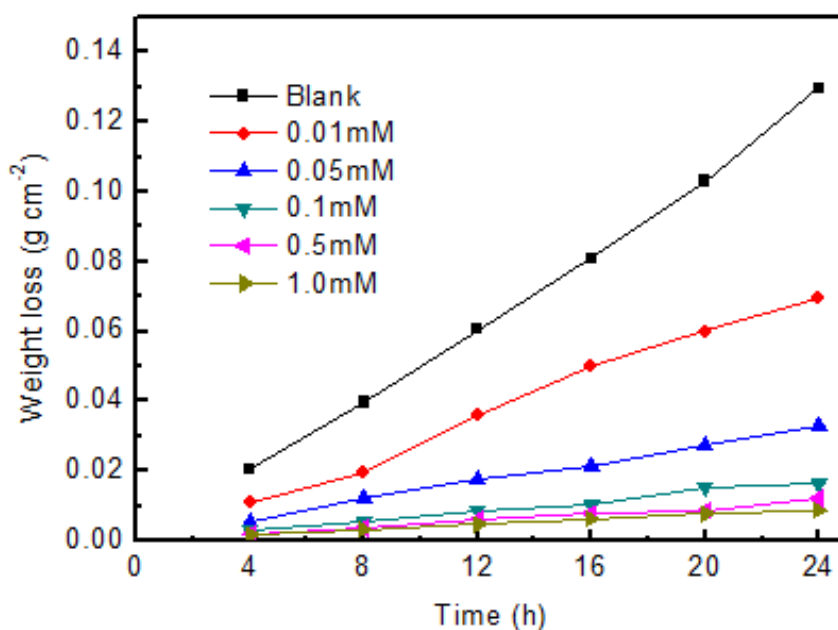


Figure 5. Variation of weight loss with time for the corrosion of mild steel in 1.0 M HCl in the absence and presence of AOBAB at 298K

3.3.2. Effect of temperature

The effect of temperature on the inhibition performance for mild steel in 1.0 M HCl solution in the absence and presence of different concentration of AOBAB at temperature range 308K~328K after 4 h immersion was obtained by weight loss measurements. The results were given in Table 5. It is evident from Table 5 that the corrosion rate decreases with increasing inhibitor concentration but increases more rapidly with rise in temperature. The increase in temperature may cause the increase of conductance of aqueous medium and thus increases the diffusion rate of hydrogen ions on the metal surface [24]. Table 5 also shows that in the studied temperature range the values of IE_w (%) increase with increasing temperature.

It can be inferred that with an increase in temperature, the adsorption equilibrium of AOBAB molecules on steel surface shifts towards the adsorption process, leading to a higher surface coverage. These results confirm that AOBAB is excellent inhibitor for corrosion of mild steel in 1.0 M HCl solutions in the studied temperature range.

The apparent activation energies (E_a) for the corrosion process were calculated from Arrhenius type plot according to the following equation:

$$\ln CR = -\frac{E_a}{RT} + A \quad 7$$

Where CR is corrosion rate, E_a is the apparent activation energy of the corrosion process, R is the universal gas constant, A is the Arrhenius pre-exponential factor and T is the absolute temperature.

Table 5. Corrosion rate of mild steel and inhibition efficiency for various concentrations of AOBAB in 1.0 M HCl at different temperature obtained from weight loss measurements.

Temp. (K)	Conc. (mM)	Corrosion rate (mg cm ⁻² h ⁻¹)	η (%)	θ
308	Blank	9.79	—	—
	0.01	4.12	57.9	0.579
	0.05	2.47	74.8	0.748
	0.1	1.21	87.6	0.876
	0.5	0.80	91.8	0.918
	1.0	0.69	92.9	0.929
318	Blank	17.8	—	—
	0.01	6.71	62.3	0.623
	0.05	3.26	81.7	0.817
	0.1	1.87	89.5	0.895
	0.5	1.32	92.6	0.926
	1.0	1.05	94.1	0.941
328	Blank	32.1	—	—
	0.01	10.5	67.3	0.673
	0.05	4.97	84.5	0.845
	0.1	2.98	90.7	0.907
	0.5	1.64	94.9	0.949
	1.0	1.32	95.9	0.959

Arrhenius plots of the logarithm of the corrosion rate obtained by weight loss measurement versus $1/T$ for blank and different concentrations of AOBAB were shown in Fig. 6. The values of E_a obtained from the slope of Arrhenius lines were given in Table 6. It is found that values of E_a for inhibited solutions are lower than that for uninhibited solutions. This decrease of apparent activation energy may be attributed to slow rate of inhibitor adsorption with a resultant closer approach to equilibrium during the experiments at higher temperature [25]. Previous studies have shown that, unchanged or lower values of E_a in inhibited systems compared to the blank have been reported to be indicative of chemisorption mechanism, while higher values of E_a suggest a physical adsorption mechanism [26]. Therefore, it can be inferred that AOBAB exerts its inhibition effects through chemisorption on the metal surface.

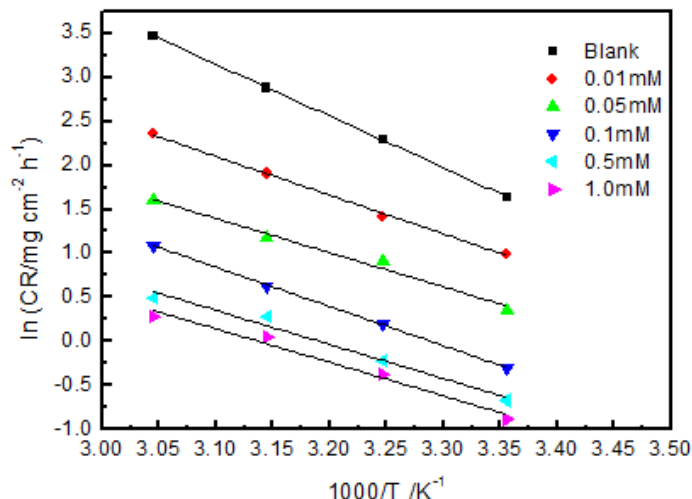


Figure 6. Arrhenius plots of $\ln (CR)$ vs. $1000/T$ for mild steel in 1.0 M HCl in the absence and presence of different concentrations of AOBAB.

An alternative formulation of Arrhenius equation is:

$$CR = \frac{RT}{Nh} \exp\left(\frac{\Delta S^*}{R}\right) \exp\left(\frac{-\Delta H^*}{RT}\right)$$

8

Where CR is corrosion rate, h is the Plank’s constant, N is Avogadro’s number, R is the universal gas constant, ΔS^* is the entropy of activation, ΔH^* is the enthalpy of activation and T is the absolute temperature. Fig. 7 shows a plot of $\ln (CR/T)$ versus $1000/T$. Straight lines were obtained with a slope of $-\Delta H^*/R$ and an intercept of $\ln (R/Nh) + \Delta S^*/R$, from which the values of ΔS^* and ΔH^* were calculated and also listed in Table 6.

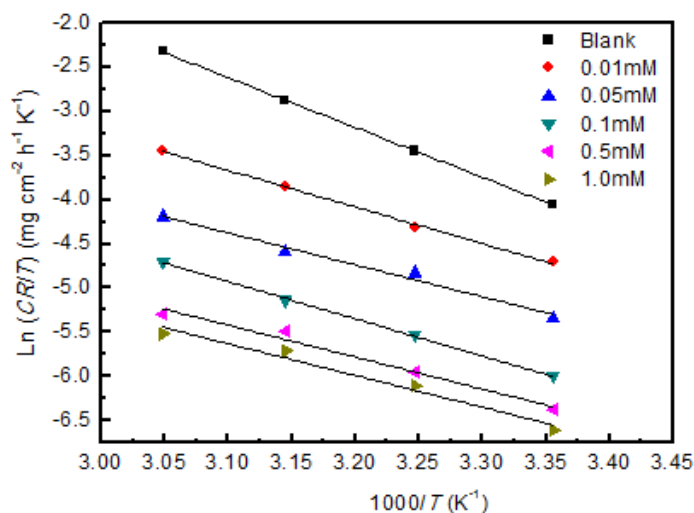


Figure 7. Arrhenius plots of $\ln (CR/T)$ vs. $1000/T$ for mild steel in 1.0 M HCl in the absence and presence of different concentrations of AOBAB.

The values of ΔH^* ranged from 46.85 to 29.89 kJ mol⁻¹, indicating the endothermic nature of the steel dissolution process. The values of ΔS^* decrease gradually with increasing AOBAB concentrations in 1.0 M HCl (except for the concentration of 0.1 mM) which implies that the activated complex in the rate determining step represents an association process rather than a dissociation step, meaning that a decrease in disordering takes place on going from reactants to the activated complex by the formation of stable adsorption layer of the AOBAB molecules on mild steel surface.

Table 6. The calculated thermodynamic parameters of adsorption (apparent activation energy (E_a), enthalpy (ΔH^*) and entropy (ΔS^*) from weight loss measurements

Conc. (M)	E_a (kJ mol ⁻¹)	ΔH^* (kJ mol ⁻¹)	ΔS^* (J mol ⁻¹ K ⁻¹)
Blank	48.92	46.85	-74.07
0.01 mM	36.64	34.44	-121.27
0.05 mM	32.31	30.06	-140.72
0.1 mM	37.07	34.91	-130.30
0.5 mM	32.24	30.05	-149.41
1.0 mM	31.65	29.89	-151.67

3.4. Adsorption isotherm

In order to get more information about the interaction of the studied inhibitor and metal surface at different temperatures, The values of surface coverage (θ) obtained from weight loss measurement at different concentrations of AOBAB in 1 M HCl in the temperature range (298-328K) after 4h immersion were used to investigate the adsorption characteristics of the inhibitor. Four widely used adsorption isotherms (Langmuir, Temkin, Frumkin and Freundlich) were tested for their fit to the experimental data. The best fit was obtained with Langmuir's adsorption isotherm, given by Equation as following:

$$\frac{C_{inh}}{\theta} = \frac{1}{K_{ads}} + C_{inh} \quad 9$$

Where θ is the degree of surface coverage, C_{inh} is the inhibition concentration in the electrolyte and K_{ads} is the equilibrium constant of the adsorption process. Plots of C/θ versus C yield a straight line as shown in Fig. 8. In both cases the linear regression coefficients (R^2) are almost equal to 1 and the slopes are very close to 1, indicating that the adsorption of AOBAB in 1.0 M HCl follows the Langmuir isotherm and exhibit single-layer adsorption characteristic. The equilibrium adsorption constant, K_{ads} , for the adsorption of the compound at different temperature were calculated from the slopes of straight lines and listed in Table 7. The increase in values of K_{ads} with increasing temperature suggested that the elevated temperature facilitates the adsorption of AOBAB. The high value of K_{ads} indicates that the AOBAB inhibitor possess strong adsorption ability onto the mild steel surface.

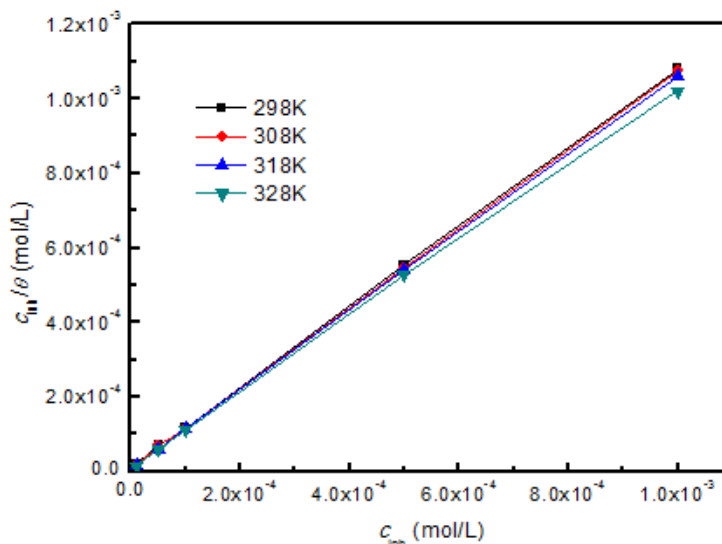


Figure 8. Equilibrium constant and standard free energy of adsorption of mild steel in 1.0 M HCl in absence and presence of different concentrations of AOBAB at different temperatures.

K_{ads} values are also related to the standard free energy of adsorption, ΔG_{ads}^0 , with the following equation:

$$K_{\text{ads}} = \frac{1}{55.5} \exp\left(\frac{-\Delta G_{\text{ads}}^0}{RT}\right) \quad 10$$

Where R is the universal gas constant and T is the absolute temperature. The value 55.5 in the above equation is the concentration of water in solution in mol L^{-1} . The values of ΔG_{ads}^0 were also listed in Table 7. The negative values of ΔG_{ads}^0 suggest that the adsorption of AOBAB is a spontaneous process. Generally speaking, values of ΔG_{ads}^0 up to -20 kJ mol^{-1} indicate the electrostatic attraction between the charged metal surface and charged organic molecules in the bulk of the solution (physisorption). Those around -40 kJ mol^{-1} or smaller involve charge sharing or charge transfer between the metal and the organic molecules (chemisorption) [27]. In this case, the calculated values of ΔG_{ads}^0 for AOBAB were ranged from -37.80 to $-42.71 \text{ kJ mol}^{-1}$. Based on the previous literatures [28], the values of ΔG_{ads}^0 indicate that adsorption of AOBAB on the mild steel surface may involve complex interactions: predominant physisorption and weak chemisorption. The conclusion can also be verified from analyzing the molecular structure of AOBAB. Generally speaking, when mild steel was immersed in the HCl solution, chloride ions are adsorbed to the metal surface, forming interconnecting bridges between the metal atoms and the positive ion (N^+) in molecule of AOBAB. Therefore, the inhibitor molecules were firstly adsorbed on metal surface by electrostatic attractions (physisorption). Afterword, The relative strong coordinate covalent bonds can be formed by transference of electrons from active sites of pre-adsorbed AOBAB molecule such as lone sp^2 electron pairs present on O atoms, π -electrons of aromatic rings as well as the double bonds to the vacant d orbitals of iron surface atoms (chemisorption).

Table 7. Adsorption parameters obtained from weight loss measurements for the studied compound in 1M HCl at different temperature.

Temp. (K)	K_{ads} ($\times 10^4 M^{-1}$)	ΔG_{ads}^0 (kJ mol $^{-1}$)	Slope	R^2
298	7.6	-37.8	1.07	0.999
308	10.6	-39.9	1.07	0.999
318	11.1	-41.3	1.05	0.999
328	11.4	-42.7	1.02	0.999

3.5. SEM analysis

In order to observe the changes in surface morphologies of corrosive samples before and after the addition of inhibitor, SEM was used. Fig. 9 presents the SEM photographs of the mild steel specimens before and after the immersion in 1.0 M HCl solution for 4 h in the absence and presence of various concentrations of AOBAB at 25°C. It can be observed from Fig. 9 (a) that the mild steel specimen before immersion seems smooth and flat, and some polishing scratches can also be seen in the surface. Inspection of Fig. 9 (b-d) reveal that the surface was damaged severely in the absence of inhibitor, while in the presence of the inhibitor, the extent of corrosion was much less. These observations confirm that the steel surfaces were covered with the inhibitor molecules and the protective inhibitor layers were formed.

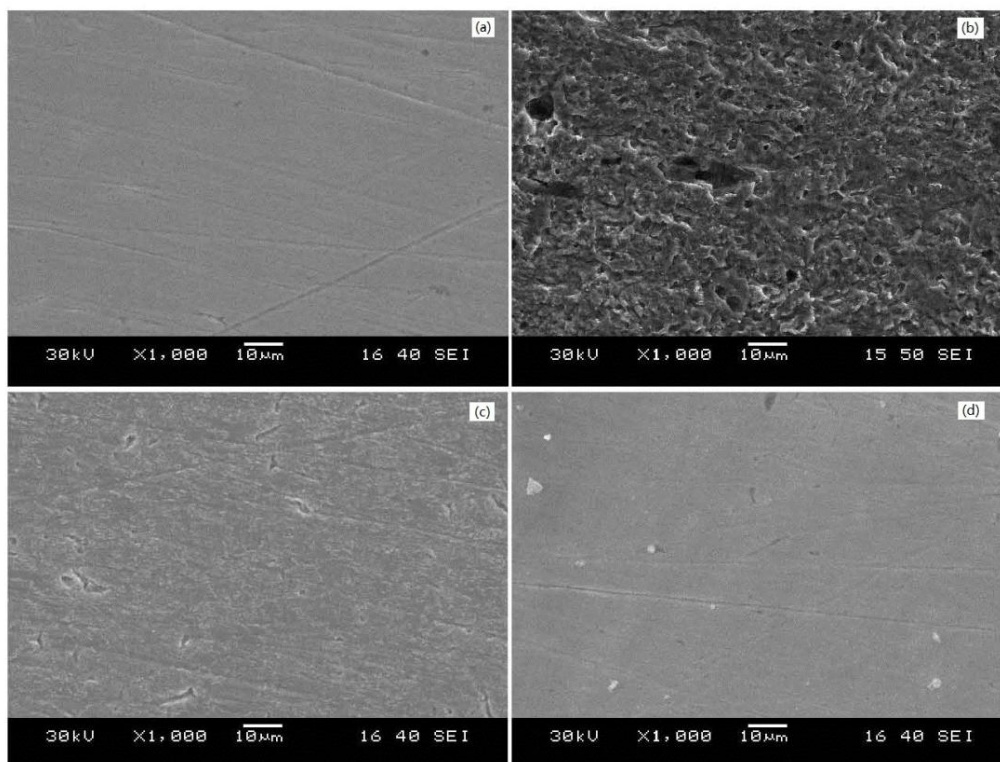


Figure 9. SEM micrographs of mild steel samples (a) only surface polishing, (b) after immersion in 1.0 M HCl solution without inhibitor, (c) after immersion in 1.0 M HCl solution in presence of 0.1 mM AOBAB, (d) after immersion in 1.0 M HCl solution in presence of 1 mM AOBAB

4. CONCLUSIONS

From the above results and discussion, the main conclusions can be summarized in the following points:

1. A new Benzopyranone derivative was synthesized and characterized by FTIR and ^1H NMR spectroscopy.
2. Results obtained from the experimental data shows that AOBAB is effective inhibitor for the carbon steel corrosion in 1.0 M HCl solutions in the investigated temperature range and its inhibition efficiency increases with the increase in its concentration and increase in temperature.
3. AOBAB acts as mixed type inhibitor.
4. The adsorption of AOBAB on the mild steel in 1.0 M HCl solutions obey Langmuir adsorption isotherm. The negative values of free energy of adsorption indicated that the adsorption of AOBAB molecule is a spontaneous process.
5. The results obtained from weight loss measurements, Tafel polarization curves and EIS are in reasonable agreement.

ACKNOWLEDGEMENTS

The authors are pleased to acknowledge the financial support provided by Specialized Research Fund for the Doctoral Program of Higher Education, China (No. 20093219120014) and NUST Research Funding, China (No. 2010ZYTS016).

References

1. J.R. Kish, N.J. Stead, D.L. Singbeil, *Corrosion* 65 (2009) 491-500
2. T. Shahrabi, H. Tavakholi, M.G. Hosseini, *Anti-Corros Method M.* 54 (2007) 308-313
3. M. Mahdavian, S. Ashhari, *Electrochim. Acta* 55 (2010) 1720-1724
4. K.F. Khaled, *Electrochim. Acta* 54 (2009) 4345-4352
5. A. Zarrouk, T. Chelfi, A. Dafali, B. Hammouti, S.S. Al-Deyab, I. Warad, N. Benchat, M. Zertoubi, *Int. J. Electrochem. Sci.* 5(5) 696-705
6. I.Ahamad, M.A. Quraishi, *Corros. Sci.* 51 (2009) 2006-2013
7. S.M.A. Hosseini, M.R. Islami, F. Mohammadi, *Asian J. Chem.* 18 (2006) 365-370
8. S.K. Shukla, M.A. Quraishi, *Corros. Sci.* 51 (2009) 1007-1011
9. A. Zarrouk, A. Dafali, B. Hammouti, H. Zarrok, S. Boukhris, M. Zertoubi, *Int. J. Electrochem. Sci.* 5(1) 46-55
10. S. Ghareba, S. Omanovic, *Corros. Sci.* 52 (2010) 2104-2113
11. I.Ahamad, R. Prasad, M.A. Quraishi, *Corros. Sci.* 52 (2010) 933-942
12. A.Popova, M. Christov, A. Vasilev, A. Zwetanova, *Corros. Sci.* 53 (2011) 679-686
13. M. Lebrini, M. Traisnel, M. Lagrenée, B. Mernari, F. Bentiss, *Corros. Sci.* 50 (2008) 473-479
14. N. Caliskan, E. Akbas, *Mater. Chem. Phys.* 126 (2011) 983-988
15. K.F. Khaled, M.N.H. Hamed, K.M. Abdel-Azim, N.S. Abdelshafi, *J. Solid State Electrochem.* (2011), article in press, DOI: 10.1007/s10008-010-1110-0
16. Z. Tao, S. Zhang, W. Li, B. Hou, *Corros. Sci.* 51 (2009) 2588-2595
17. A.A.M. Eissa, N.A.H. Farag, G.A.H. Soliman, *Bioorgan. Med. Chem.* 17 (2009) 5059-5070
18. A.Gupta, R. Sharmac, A.K. Balapurec, G. Keshrib, M.M. Singhb, S. Raya, *Lett. Drug Des. Discov.* 6 (2009) 46-50

19. M. Şahin, G. Gece, F. Karci, S. Bilgiç, *J. Appl. Electrochem.* 38 (2008) 809-815
20. E.S. Ferreira, C. Ginacomelli, F.C. Giacomelli, A. Spinelli, *Mater. Chem. Phys.* 83 (2004) 129-134
21. H. Gomez, M.K. Ram, F. Alvi, E. Stefanakos, A. Kumar, *J. Phys. Chem. C* 114 (2010) 18797-18804
22. S.K. Shukla, M.A. Quraishi, *Corros. Sci.* 51 (2009) 1990-1997
23. A.M. Toader, E. Volanschi, M.F. Lazarescu, V. Lazarescu, *Electrochim. Acta* 56 (2010) 863-866
24. K.L. Heppner, R.W. Evitts, J. Postlethwaite, *J. Electrochem. Soc.* 152 (2005) 89-98
25. S.V. Ramesh, A.V. Adhikari, *Mater. Chem. Phys.* 115 (2009) 618-627
26. I.B. Obot, N.O. Obi-Egbedi, S. A. Umoren, E. E. Ebenso, *Int. J. Electrochem. Sci.* 5 (2010) 994-1007
27. I.B. Obot, N.O. Obi-Egbedi, *Corros. Sci.* 52 (2010) 198-204
28. M.S. Morad, A.A.O. Sarhan, *Corros. Sci.* 50 (2008) 744-753